Seismic and Thermal Characterization of a Bottom Simulating Reflection in the Northern Gulf of Mexico

D.R. Hutchinson[1], P.E. Hart[2], C.D. Ruppel[3], F. Snyder[4], and B. Dugan[5]

[1] USGS, 384 Woods Hole Rd., Woods Hole, MA 02543
[2] USGS, 345 Middlefield Rd, MS 999, Menlo Park, CA 94025
[3] Georgia Tech, School of Earth and Atmospheric Sciences, Atlanta, GA 30332
[4] Schlumberger, 3600 Briarpark Dr., Houston, TX 77042
[5] Rice University, Department of Earth Sciences, MS-126, Houston, TX 77005

Abstract

High-resolution multichannel seismic reflection data, exploration industry 3D seismic data, and heat flow measurements collected on the southeast side of a minibasin (Casey basin) in the northern Gulf of Mexico continental slope have been used to characterize a bottom simulating reflection (BSR). The BSR, which covers a small area of about 15 km^2, is identified by cross cutting relationships with seismic stratigraphy. Two mounds are identified; the larger Alpha mound is structurally formed at the junction of three arms of the structural high east of the minibasin. The smaller Beta mound may be a seep site. Conventional heat flow measurements yield higher gradients (39-49 mK/m) to the northeast of the structural high and lower values (30-38 mK/m) to the south and west along the edge of the minibasin, which is separated from the structural high by the eastern Casey fault zone. When the near-seafloor thermal gradients are extrapolated to the depth of the BSR, the resulting temperatures are generally too low if the BSR marks the base of the hydrate stability zone in a methane-only gas hydrate system. Plausible changes in pore water salinity or gas composition cannot account for this disparity, and thermal perturbations caused by fluid downwelling, mass wasting, or depth-dependent thermal conductivity variations might best explain the low predicted BSR temperatures. The recognition of a BSR in the study area provides geophysical evidence that a hydrate stability zone with trapped free gas at its base exists in the northern Gulf and that minibasins can be locations for finding subsurface hydrate-associated free gas and probable gas hydrate.

Introduction

The northern Gulf of Mexico (hereafter, Gulf[1]) has long been a natural laboratory for the study of surficial gas hydrate (Anderson and others, 1983; Brooks and others, 1984; MacDonald and others, 1994; Roberts and Carney, 1997). On the other hand, identifying deeper subsurface gas hydrate, especially associated with Bottom Simulating Reflections (BSRs) that might mark the presence of free gas beneath the hydrate stability zone, has proved exceedingly difficult

[1] Many researchers shorten Gulf of Mexico to "GOM", which is easily confused with the same abbreviation used for the Gulf of Maine off New England.

(Cooper and Hart, 2002; Geresi and others, 2002). The deepest subbottom sample of gas hydrate recovered in the Gulf is quite shallow, from DSDP site 618 in Orca Basin, at a depth of approximately 20 m below the sea floor in 2412 m of water (Pflaum and others, 1986). The lack of evidence for deeper BSRs or other geophysical indicators of deep gas hydrate (for example, velocity anomalies or seismic blanking) has led some researchers to suggest that gas hydrates in the Gulf are only concentrated in shallow sediments over structural zones associated with faulting or enhanced fluid venting and are essentially at low to inconsequential concentrations in the intervening minibasins (Milkov and Sassen, 2001; Milkov and Sassen, 2003; Paull and others, 2005). Recent studies of pore-water geochemistry and thermal conditions near venting sites have been interpreted to indicate that even these structural zones may sometimes lack significant hydrate due to the inhibiting effects of salt and heat (Ruppel and others, 2005).

The Gulf of Mexico is also a world-class petroleum system (Nehring, 1991) that pervasively leaks hydrocarbons, including natural gas, into the water column (Whelan and others, 2005). With near seafloor pressure and temperature conditions conducive to hydrate formation and the existence of an abundant and leaky deeper source of natural gas, the elusiveness of observations and indirect indicators of deeper gas hydrate remains puzzling.

Within the last few years, a number of studies have emerged that identify BSRs on the Louisiana continental slope (Dai and others, 2004; McConnell and Kendall, 2003; Xu and others, 2004). New seismic imaging technologies, such as single-sensor (Q) data (Dai and others, 2004) and Ocean Bottom Cables (Hardage and others, in press) are also being used to identify low-amplitude discontinuous BSRs, quantify deeper hydrate, and measure elastic properties consistent with possible hydrate occurrence in the absence of a BSR. In this paper, we analyze a BSR from a minibasin on the Louisiana continental slope through a combination of high-resolution 2D and 3D multichannel seismic reflection data and heat flow measurements. This BSR is one target of a joint industry-government drilling program (Chevron Joint Industry Project, JIP) that drilled three sites in the Gulf for scientific studies of the hydrate stability zone

in spring, 2005 (Jones, 2004). The BSR we identify spans several lease blocks: KC151, KC152, and KC195.[2]

Geological Setting

The northern Gulf of Mexico has complicated seafloor morphology characterized by hummocky bathymetry produced by structural highs that separate ovoid-shaped minibasins. The seafloor morphology is the result of extensive salt tectonism and complex Pleistocene shelf progradation and retreat (Bryant and others, 1990; Salvador, 1991; Suter and Berryhill, 1985). Terrigenous siliclastic deposition during the Pleistocene and Holocene has been dominated by discharge from the Mississippi River (Winker and Booth, 2000) which has variously followed the Alaminos, Keathley, and Mississippi Canyon pathways (Bryant and others, 1990).

The minibasin that is the subject of this study is unnamed, and will be referred to as the Casey basin (Figure 1A) after KC (i.e., Keathley Canyon). The Casey basin is on the middle continental slope near the complex junction of four minibasins. Roughly circular in shape, the minibasin measures about 12 km east-west and 13 km northwest-southeast. The rim of the minibasin lies at about 1300 m but rises as shallow as 1210 m on the southeast edge. The basin opens to the south with a faulted sill at 1460 m. The floor of the basin is only slightly deeper than the sill at 1470-1480 m water depth, suggesting that the basin has limited ability to trap additional sediments and continue filling. Total relief of the minibasin is variable but typically measures about 150 m. The minibasins in this region are surrounded by curvilinear faults that are most easily identified on a slope map computed from bathymetric data (Figure 1B). The fault zone on the east side of the Casey basin, here called the eastern Casey fault zone, is clearly visible in both the slope and bathymetric maps (Figures 1B, 1C). The edges of the minibasin dip at only a few degrees although at the faults, relief is locally steep and complicated. This morphology of the minibasin is typical of salt-withdrawal minibasins in this part of the Gulf (Bryant and others, 1990).

[2] The U.S. Minerals Management Service divides the continental margin of the Gulf of Mexico into approximately 1°x 2° protraction areas that are further divided into approximately 4.3 km x 4.3 km numbered lease blocks. The three lease blocks comprising the study area of this paper are in the Keathley Canyon (KC) protraction area.

A pyramid-shaped mound, here called Alpha mound, about 1.5-2 km across, sits at the southeast corner of Casey basin with its apex at about 1210 m water depth (Figure 1C). Morphologically similar mud volcanoes and mounds are well mapped and studied in other parts of the northern Gulf (Kohl and Roberts, 1995; Roberts, 2001; Sager and others, 2003) and sometimes show evidence of hydrocarbon venting (Roberts and Carney, 1997; Sager and others, 2004). At the Alpha mound, faults on the eastern side disrupt and control mound morphology and indicate that faulting has post-dated mound formation. A smaller mound, here called the Beta mound, lies near the Alpha mound, but is separated from it by the eastern Casey fault zone (Figure 1C).

Data

The high-resolution 2D multichannel seismic data were collected in May, 2003, aboard the R/V Gyre (Hutchinson and Hart, 2003). A Generator-Injector[3] pneumatic airgun with dual 13 in^3 chambers provided the seismic source. Signals from the source were sensed by a 240-m-long, 24-channel, solid core streamer array and recorded at 0.5 ms sampling rate to travel times of 5 - 6 s, depending on recording delays. With a firing interval of 20 m and a channel spacing of 10 m, common depth points (CDPs) were 5 m apart with 6-fold multiplicity. All data were processed through stack and time migration during the cruise, although final editing, stacking, and migrations were completed after return to shore. Navigation was by differential Global Positioning System (DGPS); all CDP locations were corrected for antenna offset.

For the Casey basin region, approximately 600 km of data were collected in 59 lines (Hart and others, 2005; Hutchinson and Hart, 2003). A regional grid of lines spaced 1 km apart was augmented by more closely spaced lines at 500-m and 100-m spacing. Line locations were centered on the southeastern portion of the Casey basin and the structural high bounding it on the east. Interpretations of the BSR were converted to depth using stacking velocities from a 3D multichannel seismic survey collected in the region and processed by Schlumberger for the JIP project (Dai and others, 2004; Snyder and others, 2004; Xu and others, 2004). In this paper we focus on three lines that cross the minibasin and structural high in different orientations: Line

[3] Generator-Injector Guns (GI guns) are manufactured by Seismic Systems, Inc. Use of trade names is for descriptive purposes only and does not imply endorsement by the U.S. Government.

KC01 (east-west, Figure 2), Line KC11 (north-south, Figure 3), and Line KC57 (northeast-southwest, Figure 4).

Conventional 3D multichannel seismic data were collected using an 8-km-long streamer with airgun arrays totaling 5200 in^3. Only the top 4 seconds (s) were used in this study. Initial data processing utilized conventional processing at about 53-fold. Specialized reprocessing including prestack time migration at higher resolution was performed to identify potential hydrate indicators (Dai and others, 2004; Snyder and others, 2004; Xu and others, 2004).

Heat flow data were acquired in August 2003, also aboard R/V Gyre, in pogo-probe mode utilizing the Dalhousie University heat flow probe, consisting of a 6-m-long barrel with up to 32 thermistors. A single measurement consisted of a bottom water temperature record, an interval of thermal equilibration in the sediments to constrain raw sediment temperature, and then a thermal conductivity interval during which the decay of a controlled heat pulse was monitored. The product of the gradient and thermal conductivity yields heat flow. Thirteen successful measurements were completed along seismic lines KC01, KC11, and KC57 (Table 1). The locations of the heat flow measurements relative to seafloor features and the seismic data are shown in Figures 2 through 4. No seafloor transponder net was deployed for these measurements, and the exact positions of the heat flow measurements on the seafloor could be mislocated by up to 100 m or possibly more, due to the ship's navigation and movement during data acquisition, ocean currents, and deviations from linearity of the cable used to deploy the heat flow probe.

Results

Seismic stratigraphy: The seismic stratigraphy is closely correlated with the regional morphology, in which the minibasin has one seismic character and the adjacent structural high has another (Figure 2). The Casey basin consists of a generally smooth seafloor underlain by continuous reflections or reflection packages separated by unconformities. Some of the reflection packages are well laminated; others have less coherent structure and continuity. Reflectivity can be either high or low, and units can thicken into the basin (e.g., fan shaped) or be more uniformly thick (e.g., hemipelagic drape). The most prominent unconformity ("U" on Figure 2) is

continuous from about 150 ms beneath the seafloor (CDP 1800 on Figure 2) to more than 500 ms near the center of the minibasin. The BSR occurs exclusively in the units below “U” in Figure 2. Within the center of the basin, however, the BSR, if present, would be parallel to “U” and thus difficult to interpret. The multiple unconformity-bound units are consistent with stratigraphy identified in other upper and mid-slope basins (e.g., (Prather and others, 1998; Winker and Booth, 2000)) in which the numerous fan, turbidite, mass wasting, and hemipelagic units alternate in response to changing sea-levels and positions of the ancestral Mississippi drainage and shelf-edge deltas.

In contrast, the seismic stratigraphy beneath the structural high is disrupted and discontinuous (Figures 2, 3, and 4). The structural high consists of three bathymetric arms: one extending north along the eastern edge of the minibasin (North Arm on Figure 1B), one extending east (East Arm on Figure 1B), and a small segment that extends southwest to partially block the southern end of Casey basin (South Arm on Figure 1B). These three bathymetric regions contain rough topography and numerous lineations indicating fault offsets. Numerous steep faults are spaced on average 100-300 m apart and separate stratigraphic slices that are sometimes rotated and internally deformed (e.g., CDP 1850-1950 on Line KC57, Figure 4). Fault intersections suggest the presence of flower structures (e.g., CDP 1700 – 1900 on Line KC11, Figure 3) and thus a component of strike-slip motion. Relief of the seafloor is often steep, with seafloor offsets typically about 50 m but sometimes up to 100 m, creating overlapping, out-of-plane seafloor reflections, rendering identification of the sea floor reflector difficult (e.g., CDP 1600 – 1750 on Line KC01) and suggesting that faults may still be active. The rugged relief and the crossing, out-of-plane reflections in the top 100 ms (~80 m) also make interpretation of the shallow stratigraphy ambiguous. Deeper reflections (i.e., from 100 ms to greater than 500 ms subbottom, or about 80 - 400 m subbottom) show identifiable, but faulted horizons and layers with many offsets. It is not possible to correlate these deeper events with the more continuous layering in the adjacent (Casey) basin. The BSR appears to cross the faults bounding the structural high without disruption (CDP 1700-1750 on KC01, Figure 2) and extends a small distance beneath the structural high.

Within the structural high, three additional features can be identified. The first, Alpha mound, is at the intersection of the three arms of the structural high, where faulting is extremely complicated. The mound is elongated in a northwest-southeast direction, measuring about 2 km long by about 1 km wide. The northeast side of the mound is defined by the east Casey fault zone; water depths across the fault increase by 50 – 100 m. The uppermost sediments, 100 – 150 ms (~120 m) are mostly transparent or only weakly reflective. The deeper seismic stratigraphy beneath the mound contains numerous reflection packages showing general continuity of reflections, separated by faults (e.g., CDPs 1850 – 1950 of Line KC57, Figure 4). The seismic data across the mound do not image a vertical amorphous or acoustically transparent region that could be interpreted as a conduit or gas chimney.

The second feature, a small mound here called Beta mound (Figure 1C), is about 500 m northeast of Alpha mound, close enough to appear as though it is a part of Alpha mound. It is treated as a separate morphologic feature for two reasons: it is separated from the larger mound by multiple faults of the eastern Casey fault zone, and, unlike Alpha mound, there are no deeper reflections that can be traced underneath the Beta mound (near CDP 1500, Figure 2).

A small basin recognized east of Beta mound contains layered continuous reflections in the top 200 – 300 ms (~160-240 m) underlain by a faulted, sometimes discontinuous and chaotic deeper reflection fabric (CDP 900-~1450, line KC01, Figure 2). Bright spots possibly indicative of trapped free gas are frequent between 2.0 and 2.3 s. A vertical nonreflective zone 200 - 250 m wide (CDP 1100 – 1150 on Line KC01) is similar to the reflection character of a gas chimney. A BSR may exist in this section (e.g., CDPs 1200 – 1400 on Line KC01), but it can be identified only occasionally because of interference from bright spots and the complicated reflection events marking the transition to the deeper chaotic unit. There are insufficient line crossings to map the lateral extent of this potential BSR reflection within this small basin, nor is it possible to match reflection patterns from this small basin with the stratigraphy in the larger Casey basin to the west.

A deep reflection mapped in the area around Alpha and Beta mounds is interpreted as top-of-salt and occurs as a bright normal polarity reflection that has ragged intervals with

occasional steep relief (Figure 5A). It has been mapped from slices of the 3D proprietary data to maximum two-way travel times of 4.0 s (Figure 6B). The top of salt is visible on the 3D data only in the vicinity of the structural high because in other areas it exceeds 4 s. The shallowest extent of the salt is northeast of the eastern Casey fault zone where the top of an anticlinal-shaped bulge is about 2.92 s. The top of the Alpha mound and the eastern Casey fault zone occur at a saddle in the salt surface at about 3.4 s, with shallower salt occurring both northeast and southwest of the top of the mound. This relationship suggests that the saddle coincides with and may have contributed to focusing a zone of weakness and faulting. The top-of-salt surface is irregular with additional dips and rises before it deepens along the edges of the adjacent minibasins. Although the data coverage in this map is limited, it shows that the salt shoals beneath the structural high, but in a complicated geometry with no exact correlation between local sea-floor highs and salt highs. Even at its shallowest point in the northeast portion of the mapped region, the top-of- salt surface lies greater than 1.0 s travel time (~1.0 km) beneath the sea floor.

BSR: The BSR can be identified by its typical BSR character (Figures 2, 3, 5 and 7); it is subparallel to the sea floor; it cross cuts other reflections; it is immediately underlain by occasional bright reflections. These features are commonly observed in hydrate provinces with a BSR, such as Blake Ridge (Dillon and others, 1994; Dillon and others, 1992) and Hydrate Ridge (Bangs and others, 2005; Trehu and others, 2004a; Trehu and others, 2004b). The BSR is more easily identified on dip lines (east-west) where its cross-cutting geometry is most evident. On north-south lines, the BSR is more subtle and difficult to identify (Figure 3). It is generally not a high-amplitude event compared to other reflections in the minibasin or compared to BSRs from regions of hydrate occurrence outside of the Gulf. Like other BSRs, it appears to have reverse polarity (red) compared to the seafloor reflection (black) (Figures 2, 6). The strongest amplitudes occur beneath the structural high where the BSR appears to flatten beneath the seafloor, perhaps creating a geometry more conducive to trapping deeper free gas and returning stronger seismic reflections (Figure 7). At bounding faults, the BSR crosses into the structural high without apparent disruption (Figure 6), although higher amplitudes at these faults (Figure 7) suggest the faults may have acted to focus trapped gas. The more chaotic reflection character of the structural high makes it difficult to trace the BSR with any confidence for any distance

eastwards, although it may be present in the small basin identified in the East Arm of the structural high (CDP 1200 – 1300, Figure 2). To the west towards the middle of Casey basin, the BSR is impossible to identify where it becomes subparallel to both the minibasin floor and subbottom reflections.

The mappable extent of the BSR covers an irregularly shaped region about 6 km long by 3 km wide, or approximately 18 km^2 in the southeast corner of Casey basin (Figure 7). It deepens from about 1560 m in the east to about 1880 m in the west, and follows the shape of the minibasin seafloor. Its irregular shape in map form is partially due to the difficulties of identifying the BSR near its edges, especially in the deeper parts of the minibasin where it becomes subparallel to the regional stratigraphy. Assuming that the BSR marks the base of the hydrate stability zone (BHSZ) and the seafloor marks the top of the hydrate stability zone, then the thickness of the zone of potential hydrate occurrence varies from about 250 m in the east to about 440 m in the west. The dip of the BSR is therefore only a few degrees over the several kilometers distance of thickening.

Thermal Gradients: The conventional heat flow measurements collected on and around the Alpha mound (Figures 1C and 8) were processed to determine thermal gradients. Gradient values (Table 1) vary from a minimum of 28.90 ± 0.46 mK/m (penetration HF2) to a maximum of 49.40 ± 0.46 mK/m (penetration HF1), representing an increase of 70%. These adjacent stations are ~415 m apart and show the largest changes in thermal conditions over the shortest baseline in the survey area.

The quality of the gradient data is generally excellent. For half of the penetrations, the error is estimated at less than 1 mK/m; for the rest, the error is 1 - 2 mK/m except for Station 7, which has the largest error of 3.05 mK/m. The shape of the gradient curves is consistently linear suggesting that the sediments are in conductive thermal equilibrium and disturbances by bottom water temperature variations are minimal. The gradient deviates from linearity in the top 1 – 1.5 m on a few of the penetrations (e.g., stations HF6, HF9, and HF11). This deviation may be the result of near-surface effects (e.g., recent changes in bottom water temperatures, local advective

processes, possibly including bioirrigation, or variations in local sedimentation rates). There is little evidence in the gradient data for nonuniformities (concavity) that might indicate advective fluid transfer.

The thermal gradients can be geographically separated into two regions (Figure 8); the lowest values (30 - 34 mK/m) roughly coincide with the Alpha mound; the highest values (39-49 mK/m) are outside the mound in deeper portions of the structural high (all three arms) and along the edge of the Casey basin. One anomalous measurement outside of the mound (HF2) has the lowest gradient measured (28.9 mK/m), but is close (about 220 m) to the mound. The eastern Casey fault zone separates the low gradient values on the mound from the higher gradient values to the northeast. To the west and south, we have only two measurements outside the Alpha mound (HF4 and HF10), and the thermal gradients for these stations are both ~38mK/m, or slightly higher than the gradients measured on the Alpha mound. We include these two stations with the mound values, recognizing that we have insufficient measurements to determine whether this area actually has thermal conditions transitional between the mound and the region to the northeast.

Discussion

Identification of a BSR in the Keathley Canyon area of the northern Gulf of Mexico adds to the small but growing list of BSRs identified in this marine environment (Cassassuce and others, 2004; McConnell and Kendall, 2003). The geographic extent of the BSR presented here is small (~18 km^2), although the true extent is difficult to assess because of the ambiguity in identifying the BSR at its mapped edges, where the complicated stratigraphy obscures the BSR or the BSR becomes subparallel to the regional seismic stratigraphic trends. The existence of a BSR provides definitive geophysical evidence that a hydrate stability zone with trapped free gas at its base can occur in the northern Gulf and that minibasins can be locations for subsurface hydrate-associated gas and probably gas hydrate.

The emerging integrated geological picture that emerges suggests that the Casey basin is a subsided basin mostly filled to the level of its sill. Based on the geometries of reflection packages above unconformity U (Figure 2), which thicken toward the basin center, subsidence may still be occurring. Adjacent to and east of the minibasin is a deforming structural high with a faulted and overall much more complicated seismic stratigraphy. Within the structural high, steep seafloor slopes appear to be fault controlled and indicate that some of this region may also still be actively deforming. This geological framework is consistent with the general geological evolution of minibasins in the Gulf (Prather and others, 1998; Salvador, 1991; Winker and Booth, 2000).

The Alpha mound, which occurs at the intersection of the three arms of the structural high, is at the larger end of the spectrum of similar sized and shaped mounds identified elsewhere in the Gulf (Roberts and Carney, 1997; Sager and others, 2003). Like these mounds, the Alpha mound is structurally controlled, with its development and morphology produced by faulting, in this case faulting at the intersection of the three arms of the structural high. However, the continuity of the deeper reflections, albeit intensely faulted beneath the mound, and the absence of acoustically transparent or “blank” zones at depth suggest that the mound is not an active seep. This does not preclude the possibility that such a vent might lie in the region between the seismic lines, only that such a vent is smaller than the 100-m to 500-m line spacing, and is not likely to have played a primary role in the formation of this large mound. The Alpha mound may be an end-member in mound development in the Gulf, in which faulting without focused fluid flux is the dominant process of formation.

The Beta mound, in contrast, is much smaller and has vertical acoustically transparent zones, no clear continuous deeper reflections, and a chimney structure occupying the width of the mound, similar to the seismic character observed at other seep sites/mounds in the Gulf of Mexico (Roberts, 2001; Roberts and Carney, 1997; Sager and others, 1999; Sager and others, 2003). It is much smaller than the Alpha mound and separated from it by the eastern Casey fault zone. This smaller Beta mound could be an active or fossil seep site. Unfortunately, the heat flow measurements are not located directly on the mound, nor do we have any direct observations of the seafloor at this site.

The eastern Casey fault zone separates two distinctly different geologic regimes. East of the fault zone, there are multiple seismic indicators of shallow gas: bright reflections, vertical wipe-outs, and a potential seep site (Beta mound). The thermal gradients also change abruptly across the fault from values of 30-34 mK/m on the Alpha mound to more than 40 mK/m east of the fault. Salt also becomes shallower beneath the East Arm. When combined, these data suggest the eastern Casey fault zone separates a warmer, potentially saltier region with shallow gas occurrence and at least some sites of fluid flux on the east from a cooler region of diffusive, conductive processes to the west, within the Casey basin and on the South Arm of the structural high. Increased heat flow and salt concentrations would limit formation of hydrate and allow accumulation of free gas. To the extent that the position of the heat flow probe on the seafloor is known, it appears that one measurement along the fault (HF7) has the highest degree of variability from thermistor to thermistor while another measurement (HF1) yields a highly linear gradient with littler inter-thermistor variability. A variety of fault-related processes might contribute to the noisy nature of the data at HF7.

The thermal data are in general consistent with other measurements in the northern Gulf. Whereas older reports show gradients less than 38 mK/m (Epp and others, 1970; Jones and others, 2003), more recent experiments show that thermal gradients in the vicinity of fluid venting sites are larger by a factor of more than 10, reaching 557 +/- 5.2 mK/m at GB425 and 435 +/- 43 mK/m at MC852 (Ruppel and others, 2005). The heat flow values calculated in our Keathley Canyon study, which range from 36.2 mW/m^2 to 56.6 mW/m^2 (Table 1), are well within the range of regional heat flow values in the northern Gulf, reported as 13.4 – 80.3 mW/m^2 (Jones and others, 2003).

The near-seafloor thermal measurements can be used to investigate conditions of the gas hydrate reservoir by extrapolation of measured thermal gradients to the depth of the BSR to estimate temperatures (Table 2). Depths to the BSR were been mapped using proprietary 3D data (Snyder and others, 2004; Xu and others, 2004), and these values were made available at the site of each heat flow measurement[4]. Converting these depths to hydrostatic pressures, we also

[4] Figure 6 shows the amplitudes from this proprietary data set.

calculated theroretical BSR temperatures with CSMHYD (Sloan, 1998) assuming methane as the only hydrate former and various seawater salinities. Pure methane gas composition is supported by extremely high methane to ethane ratios in the nearby JIP drill core (Lorenson and others, 2005) and light ^{13}C isotopic values recovered from both piston cores (Pohlman and others, 2005) and the nearby JIP drill samples (Kastner and others, 2005).

A comparison of the temperatures estimated by extrapolating the thermal gradients to BSR depths shows that only HF4 produces a predicted BSR temperature consistent with a methane – seawater system (Table 2, Figure 9). At two other locations (HF1 and HF6), temperatures estimated from the gradient extrapolation are too high. At the rest of the stations, the temperatures estimated from the gradients are too low by 1-3°C (Figure 9). Due to the scatter in the predicted BSR temperatures, even doubling of pore water salinity, which shifts the hydrate stability curve to the left in Figure 9, does not significantly improve the fit across the entire data set. We also tested the impact of other hydrate-forming gases, most of which shift the hydrate stability conditions toward higher temperature.

The inconsistency between the extrapolated and theoretical BSR temperatures indicates that the temperatures measured in the shallow section are unlikely to truly reflect thermal conditions at depth. Similar temperature discrepancies have been noted at sites with coincident heat flow and borehole data off Vancouver Island (ODP Leg 146, (Grevemeyer and Villinger, 2001)) and on the Blake Ridge (ODP Leg 164, (Ruppel, 1997, 2000). For the two heat flow penetrations in this data set that predict BSR temperatures lying above the stability curve for methane hydrate (HF1 and HF6), the obvious explanation is that thermal gradients decrease with depth. Such nonuniform temperature gradients can be created by upward advection of heat and fluid. Both penetrations lie along the eastern Casey fault zone, where the faults likely act as key conduits for advective flux (e.g., (Wilson and Ruppel, submitted)). A similar process is inferred to occur at seeps throughout the northern Gulf (Macdonald and others, 2005; MacDonald and others, 1994; Sager and others, 2003; Sager and others, 2004).

For most of the heat flow measurements, the predicted temperatures at the BSR are significantly colder than would be expected if the BSR serves as the base of methane hydrate

stability. Most of the measurements on the Alpha mound fall into this category. If we assume that the temperature at the BSR must truly be close to the phase boundary and that the near-seafloor thermal gradients measured by conventional heat flow techniques are also reliable, then the thermal gradients must increase with depth into the sediments, again producing a nonuniform gradient. Three geological mechanisms might contribute to this phenomenon:

(1) Downward advection of seawater into the sedimentary column (Figure 10A). Downward fluid flux can be driven by deep, negatively buoyant brines that develop at the edges of salt bodies (e.g., (Ranganathan and Hanor, 1988)) or be a passive hydrologic response in bathymetric lows around irregular seafloor relief, as discussed by Wilson and Ruppel, (submitted). Using models that couple thermally and chemically driven flow, they show that downwelling over bathymetric highs above salt can persist for at least 250 ky after the emplacement of the salt dome.

(2) Recent rapid deposition event (Figure 10B). Rapid sedimentation involves emplacement of material that has a temperature equivalent to the bottom water on sediment with an already established thermal gradient. Elsewhere in the Gulf of Mexico, depositional processes are known to produce lower near-seafloor thermal gradients on the youngest deep-water fan lobe of the Mississippi River (Jones and others, 2003; Nagihara and others, 2002). The same effect can occur with mass wasting deposits that mobilize and redeposit material, for example on steep slopes or in regions of faulting throughout the Gulf of Mexico (Tripsanas and others, 2004; Twichell and others, 2000). Rapid sedimentation provides a plausible explanation for the thermal results and is also supported by carbon dating that indicates at least one age inversion in the uppermost meters of sediment on the structural high, consistent with the interpretation of mass wasting (Pohlman and others, 2005). The seismic data used in our study are not high-enough spatial or temporal resolution to show rapid depositional events of less than a few meters in dimension.

(3) An increase in temperature with depth due to thermal focusing by high thermal conductivity salt underlying the Alpha mound (Figure 10C). Considering exclusively conductive thermal processes, the presence of salt at depth has long been known to lead to heat focusing (e.g., (Yu and others, 1992a; Yu and others, 1992b)). We note, however, that the salt lies at about 1.5 km below the Alpha mound, while the BSR is at 200-300 m. If salt depth explains the

misfit, one might expect a correlation between depth (i.e., travel time) to the top of salt and the degree of temperature misfit at the BSR, but a plot of these two parameters (Figure 11) shows no simple correlation or trend. Hence, deeper salt may explain some of the temperature disparity at the BSR, although clearly not via a simple relationship.

Additional explanations for these temperature discrepancies include capillary forces in fine-grained sediments that inhibit hydrate formation (Clennell and others, 2000; Clennell and others, 1999; Francisca and others, 2005; Ruppel, 1997) or diffusion of water, gas, and salt (Henry and others, 1999). In addition, recent evidence from a borehole in the Nankai trough documents lithology-dependent variability in downhole thermal gradients over a period of 50 days and demonstrates that the average geothermal gradient was formed by segments of gradients that were both higher and lower than the background average (Fujii and others, 2005; Tripsanas and others, 2004). If similar conditions occur in the Gulf, the near-seafloor temperatures could represent a gradient slightly different from the regional average gradient.

The geologic and thermal data presented here remain to be reconciled with geochemical data, especially pore-water data on sulfide, sulfate, and methane concentrations in the shallow sediments. These species are often used as proxies for methane flux (Borowski and others, 1996; Dickens, 2001). Because the rate of chemical diffusion is much less than the rate of thermal diffusion, geochemical conditions take much longer to equilibrate and therefore are more sensitive indicators of fluid processes. Recent studies of pore-water chemistry in shallow sediments elsewhere in the Gulf are beginning to reveal the great complexity of shallow fluid processes in the Gulf (Aharon and Fu, 2003; Aharon and Fu, 2000; Joye and others, 2004; Mills and others, 2003; Mills and others, 2005; Orcutt and others, 2004).

Finally, the data presented here provide a geologic framework for understanding the JIP Keathley Canyon drilling site, which is located approximately 2 km north of line KC01 and HF4, on the eastern edge of Casey basin. The two holes, one logging-while-drilling hole and one coring hole, lie west of the eastern Casey fault zone bounding the minibasin, in the zone of inferred lower thermal gradients and in a predominantly conductive thermal environment. The BSR near the drill site appears to be confined primarily to the units beneath unconformity U

(Figure 2). The existence of a BSR is an encouraging indicator for the occurrence of subsurface marine gas hydrate and trapped free gas, similar to how the BSR has been used to identify the occurrence of hydrate in other marine environments (Kvenvolden, 1992). Finally, the seismic data indicate that the drill site should penetrate coarser (silt to fine sand) stratigraphic units within the complex sedimentary fill of the minibasin, and these coarser units are good candidates to serve as the reservoir for gas hydrate deposits within the minibasin.

Conclusions

High-resolution multichannel seismic reflection data and 13 heat flow measurements along the southeastern flank of the Casey basin in the Keathley Canyon area of northern Gulf of Mexico have been used to map and characterize potential deeper gas hydrate in this mid-slope environment. Significant results are:

- The geologic framework of the region consists of the Casey basin and an adjacent structural high to the east consisting of North, East, and South arms. Correlation of the seismic stratigraphy between the minibasin and the structural high is uncertain, especially for a small basin sitting atop the East Arm of the structural high. The eastern Casey fault zone, which is comprised of an arcuate set of fault segments, separates the minibasin from the structural high.
- A bottom simulating reflection (BSR) covers a ~15 km^2 area in the southeastern flank of the Casey minibasin. Water depths are about 1300 m, and the BSR deepens from about 250 mbsf in the east to about 440 mbsf in the west. The actual extent of the BSR may be greater because of the difficulty in identifying the BSR at its mapped edges to the east beneath the structural high and to the west beneath the middle of the minibasin. This BSR provides good geophysical evidence that a hydrate stability zone with trapped free gas at its base exists at mid-slope water depths in the northern Gulf of Mexico. This observation also suggests that minibasins are potential sites for the occurrence of deeper hydrate than that associated with surface seep sites. This result contrasts with previous work in the Gulf focusing on near-seafloor occurrence of hydrate associated with surface seeps.
- Two mounds are identified: The large Alpha mound that is structurally formed by faulting at the junction of the North, East, and South Arms of a sea floor high and the

much smaller Beta mound, which lies northeast of the Alpha mound and is separated from it by the eastern Casey fault zone. Although highly faulted and offset, reflections that make up the seismic stratigraphy of the Alpha mound can be traced beneath and across the mound. Thermal gradients are lowest beneath the Alpha mound (30 – 34 mK/m) suggesting the existence of a thermally equilibrated region in which heat is transferred to the surface primarily by conductive processes. Beneath the Beta mound, reflections are not continuous and the lack of reflectivity is consistent with the existence of a gas- or fluid-filled chimney. Hence, the Beta mound is interpreted as a seep site. Our data do not resolve whether the seep is currently active, although steep and rugged bathymetric relief in the nearby fault zone and around the mound suggest faulting is on-going.

- The thermal gradient data can be divided into two regions: higher gradients are measured northeast of the eastern Casey fault zone (39-49 mK/m), and lower gradients occur to the southwest (30-38 mK/m). The Alpha mound has the lowest gradients (30 -34 mK/m) with the exception of a measurement of 28.9 mK/m within the eastern Casey fault zone.
- Although the linear characteristics of the thermal gradient data indicate a system in thermal equilibrium, temperatures extrapolated to depths of the BSR are generally 1-3 ^{o}C lower than modeled temperatures for given depths (pressures) of the BSR in a methane-seawater system. Our data cannot resolve among three possible explanations for this discrepancy: downwelling of fluids, an increase in temperatures with depth due to thermal focusing by underlying salt, or modification of thermal regimes by mass wasting.

Acknowledgements

Support for this work was provided by USGS, the Department of Energy, and the Chevron Joint Industry Project (JIP). Myung Lee (USGS) processed and migrated the 2D multichannel seismic data. We thank WesternGeco/Schlumberger for permission to use and publish the 3D seismic images, derivative bathymetry, amplitude map of the BSR, and travel times to the top of salt. Emrys Jones provided encouragement and allowed access to unpublished JIP data. This work would not have been possible without the assistance of the crew and scientists that participated in the two R/V Gyre expeditions. This manuscript was improved by reviews by William Waite and Uri ten Brink. C.R. was on assignment at and fully supported by the National Science Foundation during completion of this project. The opinions expressed reflect those of the authors, not NSF.

Table 1: Thermal Gradients and Heat Flow Estimates

Hf #	Water depth (m)	Latitude (N) (degree)	Latitude (N) (minutes)	Longitude (degrees)	Longitude (minutes)	dT/dz mK/m	error	Conduct W/m-K	Error	HF mW/m^2	error
1	1340m	26	48.737	92	58.546	49.40	0.86	1.14	0.13	56.60	7.20
2	1310m	26	48.513	92	58.522	28.90	0.46	1.31	0.12	37.90	4.06
3	1275m	26	48.293	92	58.506	32.50	0.61	1.29	0.15	42.10	5.74
4	1330m	26	48.316	92	58.983	37.70	0.78	1.20	0.11	45.20	5.10
5	1290m	26	48.311	92	58.716	30.90	1.59	1.17	0.15	36.20	6.60
6	1285m	26	48.312	92	58.417	44.90	1.15	1.17	0.28	52.30	14.06
7	1293m	26	48.312	92	58.117	43.20	3.05	1.22	0.46	52.80	23.70
8	1260m	26	48.133	92	58.541	34.60	1.91	1.56	0.21	43.50	9.73
9	1250m	26	47.854	92	58.539	31.40	0.72	1.19	0.14	37.40	5.25
10	1298m	26	47.447	92	58.516	38.25	1.68	1.18	0.14	44.97	7.36
11	1230m	26	47.890	92	58.223	30.54	0.81	1.18	0.14	36.15	5.36
12	1295m	26	48.315	92	57.604	39.30	1.19	1.17	0.16	46.00	7.74
13	1305m	26	48.306	92	57.236	40.80	1.58	1.12	0.24	45.70	11.44

Table 2: Comparison of Estimated and Theoretical Temperatures at the BSR

HF #	Measured Gradient (mK/m)	Uncertainty (mK/m)	T at BSR using $T_{seafloor}$ =4.3°C	T minimum at BSR (°C) (includes uncertainty)	T maximum at BSR (°C) (includes uncertainty)	T (°C) CSMHYD 100% CH4 3.3% NaCl	Difference $T_{bsr/gradient}$ – CSMHYD (°C)	T (°C) due to uncertainty
1	49.4	0.86	16.6	16.42	16.85	16.16	0.5	0.2
2	28.9	0.46	12.1	11.99	12.24	16.11	-4.0	0.1
3	32.5	0.61	13.1	12.97	13.30	15.9	-2.8	0.2
4	37.7	0.78	16.4	16.10	16.60	16.32	0.0	0.2
5	30.9	1.59	14.0	13.53	14.53	16.06	-2.0	0.5
6	44.9	1.15	16.7	16.34	16.97	15.9	0.8	0.3
7	43.2	3.05	13.1	12.45	13.69	15.7	-2.6	0.6
8	34.6	1.91	15.0	14.42	15.61	15.95	-0.9	0.6
9	31.4	0.721	13.9	13.72	14.16	15.9	-2.0	0.2
10	38.25	1.68	14.8	14.30	15.22			
11	30.54	0.81	13.4	13.17	13.65			

References Cited

Aharon, P., and Fu, B., 2003, Sulfur and oxygen isotopes of coeval sulfate-sulfide in pore fluids of cold seep sediments with sharp redox gradients: Chemical Geology, v. 195, no. 1-4, p. 201-218.

Aharon, P., and Fu, B.S., 2000, Microbial sulfate reduction rates and sulfur and oxygen isotope fractionations at oil and gas seeps in deepwater Gulf of Mexico: Geochimica Et Cosmochimica Acta, v. 64, no. 2, p. 233-246.

Anderson, R.K., Scalan, R.S., Parker, P.L., and Behrens, E.W., 1983, Seep oil and gas in Gulf of Mexico slope sediment: Science, v. 222, no. 4624, p. 619-621.

Bangs, N.L.B., Musgrave, R.J., and Trehu, A.M., 2005, Upward shifts in the southern Hydrate Ridge gas hydrate stability zone following postglacial warming, offshore Oregon: Journal of Geophysical Research, v. 110, no.B3, 13 p.

Borowski, W., Paul, C., Ussler, III, and William, 1996, Marine pore-water sulfate profiles indicate in situ methane flux from underlying gas hydrate: Geology, v. 24, p. 655-658.

Brooks, J., Kennicutt, M.C., II., Fay, R.R., McDonald, T., J., and Sassen, R., 1984, Thermogenic Gas Hydrates in the Gulf of Mexico: Science, v. 225, p. 409-411.

Bryant, W.R., Bryant, J.R., Feeley, M.H., and Simmons, G.R., 1990, Physiographic and bathymetric characteristics of the continental slope, Northwest Gulf of Mexico: Geo-Marine Letters, v. 10, no. 4, p. 182-199.

Cassassuce, F., Rector, J.W., and Hoversten, M., 2004, Study of gas hydrates in the deep-sea Gulf of Mexico from seismic data: The Leading Edge, April 2004, p. 366-372.

Clennell, M.B., Henry, P., Hovland, M., Booth, J.S., Winters, W.J., and Thomas, M., 2000, Formation of natural gas hydrates in marine sediments; gas hydrate growth and stability conditioned by host sediment properties, *in* Holder, G.D., and Bishnoi, P.R., eds., Annals of the New York Academy of Sciences, vol.912: New York, New York Academy of Sciences, p. 887-896.

Clennell, M.B., Hovland, M., Booth, J.S., Henry, P., and Winters, W.J., 1999, Formation of natural gas hydrates in marine sediments 1. Conceptual model of gas hydrate growth conditioned by host sediment properties: Journal of Geophysical Research, v. 104, no. B10, p. 22985-23003.

Cooper, A.K., and Hart, P.E., 2002, Seismic Studies of the Gas Hydrate Stability Zone, Northern Gulf of Mexico: Proc. 4th International Conference on Gas Hydrates, Yokohama, May 19-23, 2002, p. 115-123.

Dai, J., Xu, H., Snyder, F., Dutta, N., and Herron, D., 2004, Detection and estimation of gas hydrates using rock physics and seismic inversion; examples from the northern deepwater Gulf of Mexico: The Leading Edge, v. 23, no. 1, p. 60-66.

Dickens, G.R., 2001, Sulfate profiles and barium fronts in sediment on the Blake Ridge; present and past methane fluxes through a large gas hydrate reservoir: Geochimica et Cosmochimica Acta, v. 65, no. 4, p. 529-543.

Dillon, W.P., Lee, M.W., and Coleman, D.F., 1994, Identification of marine hydrates in-situ and their distribution off the Atlantic Coast of the United States, *in* Sloan, E.D., Happell, J., and Hnatow, M.A., eds., NYAS Int. Conf. on Natural Gas Hydrates, p. 364-380.

Dillon, W.P., Lee, M.W., Fehlhaber, K., and Coleman, D.F., 1992, Gas hydrates on the Atlantic Continental Margin of the United States - controls on concentration, *in* Howell, D.G., ed., The Future of Energy Gases, USGS Prof Pap No 1570, p. 313 - 330.

Epp, D., Grim, P.J., and Langseth, M.G., Jr., 1970, Heat flow in the Caribbean and Gulf of Mexico: Journal of Geophysical Research, v. 75, no. 29, p. 5655-5669.

Francisca, F.M., Yun, T.S., Ruppel, C., and Santamarina, J.C., 2005, Geophysical and geotechnical properties of near-seafloor sediments in the northern Gulf of Mexico gas hydrate province: Earth and Planetary Science Letters, v. 237, p. 924-939, doi: 910.1016/j.epsl.2005.1006.1050.

Fujii, T., Nagakubo, S., Kawasaki, T., Fukuhara, M., and Fujii, K., 2005, Temperature variation in methane hydrate bearing sediments in the eastern Nankai Trough, Japan (Abs.): EOS, American Geophysical Union, p. OS42A-06.

Geresi, E., Lutken, C., McGee, T., and Lowrie, A., 2002, Complex geology and gas hydrate dynamics characterize Mississippi Canyon Block 798 on the upper continental slope of the northern Gulf of Mexico, *in* Dutton, S.P., Ruppel, S.C., and Hentz, T.F., eds., Transactions - Gulf Coast Association of Geological Societies, vol.52, p. 309-321.

Grevemeyer, I., and Villinger, H., 2001, Gas hydrate stability and the assessment of heat flow through continental margins: Geophysical Journal International, v. 145, no. 3, p. 647-660.

Hardage, B.A., Roberts, H.H., Murray, P.E., Remington, R., Sava, D., Shedd, W.W., and Hunt, J., Jr. , in press, Multicomponent seismic technology assessment of fluid-gas expulsion geology and gas hydrate systems: Gulf of Mexico: AAPG Hedberg volume, p. 46 ms. pp.

Hart, P.E., Hutchinson, D.R., and Lee, M.W., 2005, High-resolution multichannel seismic-reflection data acquired in the northern Gulf of Mexico, 2003: U.S. Geological Survey Open-File Report 2005-1411, p. http://pubs.usgs.gov/of/2005/1411/.

Henry, P., Thomas, M., and Clennell, M.B., 1999, Formation of natural gas hydrate in marine sediments 2. Thermodynamic calculations of stability conditions in porous sediments: Journal of Geophysical Research, B, Solid Earth and Planets, v. 104, p. 23,005-023,022.

Hutchinson, D.R., and Hart, P.E., 2003, Cruise report for G1-03-GM USGS Gas Hydrates cruise, R/V Gyre, 1-14 May, 2003, Northern Gulf of Mexico: US Geological Survey Open File Report 03-474, 103 p.

Jones, E.H., 2004, Pre-cruise estimates of sediment properties for the 2005 ChevronTexaco et al. Gulf of Mexico gas hydrate research coring project (abs.), *in* Natural Gas Hydrates: energy resource potential and associated geologic hazards, Vancouver, BC, Canada, AAPG Hedberg Research Conference, p. http://www.searchanddiscovery.net/documents/abstracts/2004hedberg_vancouver/short/jones.htm.

Jones, M.L., Nagihara, S., and Smith, M.A., 2003, The regional geothermal heat flow regime of the north-central Gulf of Mexico continental slope, *in* Stone, G.W., Wrenn, J.H., and Bentley, S.J., eds., Transactions - Gulf Coast Association of Geological Societies, v.53, p. 363-373.

Joye, S.B., Boetius, A., Orcutt, B.N., Montoya, J.P., Schulz, H.N., Erickson, M.J., and Lugo, S.K., 2004, The anaerobic oxidation of methane and sulfate reduction in sediments from Gulf of Mexico cold seeps, *in* Zhang, C.L., and Lanoil, B., eds., Chemical Geology, p. 219-238.

Kastner, M., Claypool, G.A., Robertson, G., Schultheiss, P., and Holland, M., 2005, Geochemical evidence for gas hydrates at Atwater Valley and Keathley Canyon, Gulf of Mexico (Abs.): EOS, American Geophysical Union, p. OS31D-03.

Kohl, B., and Roberts, H.H., 1995, Mud volcanoes in the Gulf of Mexico; a mechanism for mixing sediments of different ages in slope environments, *in* John, C.J., and Byrnes,

M.R., eds., Transactions - Gulf Coast Association of Geological Societies, vol.45, p. 351-359.
Kvenvolden, K.A., 1992, A Primer on Gas Hydrates, *in* Howell, D.G., ed., The Future of Energy Gases, US Geological Survey, p. 279 - 291.
Lorenson, T.D., Dougherty, J.A., and Claypool, G.E., 2005, Preliminary Results from the ChevronTexaco Gulf of Mexico Gas Hydrates JIP: Hydrocarbon Gases in Sediments (Abs.): EOS, American Geophysical Union,, p. OS42A-04.
Macdonald, I.R., Bender, L.C., Vardaro, M., Bernard, B., and Brooks, J.M., 2005, Thermal and visual time-series at a seafloor gas hydrate deposit on the Gulf of Mexico slope: Earth and Planetary Science Letters, v. 233, p. 45-59.
MacDonald, I.R., Guinasso, N.L., Sassen, R., Brooks, J.M., Lee, L., and Scott, K.T., 1994, Gas hydrate that breaches the sea floor on the continental slope of the Gulf of Mexico: Geology, v. 22, p. 699-702.
McConnell, D.R., and Kendall, B.A., 2003, Images of the base of gas hydrate stability in the deepwater Gulf of Mexico; examples of gas hydrate traps in Northwest Walker Ridge and implications for successful well planning: The Leading Edge, v. 22, no. 4, p. 361-367.
Milkov, A.V., and Sassen, R., 2001, Estimate of gas hydrate resource, northwestern Gulf of Mexico continental slope: Marine Geology, v. 179, no. 1-2, p. 71-83.
---, 2003, Preliminary assessment of resources and economic potential of individual gas hydrate accumulations in the Gulf of Mexico continental slope: Marine and Petroleum Geology, v. 20, p. 111-128.
Mills, H.J., Hodges, C., Wilson, K., MacDonald, I.R., and Sobecky, P.A., 2003, Microbial diversity in sediments associated with surface-breaching gas hydrate mounds in the Gulf of Mexico: FEMS Microbiology. Ecology, v. 46, no. 1, p. 39-52.
Mills, H.J., Martinez, R.J., Story, S., and Sobecky, P.A., 2005, Characterization of Microbial Community Structure in Gulf of Mexico Gas Hydrates: Comparative Analysis of DNA- and RNA-Derived Clone Libraries: Applied and Environmental Microbiology, v. 71, no. 6, p. 3235-3247.
Nagihara, S., Brooks, J.M., Bernard, B.B., Summer, N., Cole, G., and Lewis, T., 2002, Application of marine heat flow data important in oil, gas exploration: Oil and Gas Journal, v. 100, no. 27, p. 43-49.
Nehring, R., 1991, Oil and gas resources, *in* Salvador, A., ed., The Geology of North America, v. J, The Gulf of Mexico Basin: Boulder, Geological Society of America, p. 445-494.
Orcutt, B.N., Boetius, A., Lugo, S.K., MacDonald, I.R., Samarkin, V.A., and Joye, S.B., 2004, Life at the edge of methane ice; microbial cycling of carbon and sulfur in Gulf of Mexico gas hydrates, *in* Zhang, C.L., and Lanoil, B., eds., Chemical Geology, p. 239-251.
Paull, C.K., Ussler, W., III, Lorenson, T.D., Winters, W., and Dougherty, J.A., 2005, Geochemical constraints on the distribution of gas hydrates in the Gulf of Mexico: Geo-Marine Letters, v. 25, p. 273-280.
Pflaum, R.C., Brooks, J.M., Cox, H.B., Kennicutt, M.C., and Sheu, D-D., 1986, Molecular and Isotopic Analysis of Core Gases and Gas Hydrates, DSDPLeg 96: Init Repts of DSDP US Govt Print Off, Washington, D.C., v. 96, p. 781-784.
Pohlman, J.W., Ruppel, C., Hutchinson, D.R., Hart, P.E., Plummer, R., Knies, D.L., Grabowski, K.S., and Coffin, R.B., 2005, The effects of mass deposition, gas flux and salt diapirs on surface sediment geochemistry in Keathley Canyon (northern Gulf of Mexico) (Abs.): EOS, American Geophysical Union, paper OS31D-04.

Prather, B.E., Booth, J.R., Steffens, G.S., and Craig, P.A., 1998, Classification, lithologic calibration, and stratigraphic succession of seismic facies of intraslope basins, deep-water Gulf of Mexico: AAPG Bulletin, v. 82, no. 5A, p. 701-728.

Ranganathan, V., and Hanor, J.S., 1988, Density-driven groundwater flow near salt domes, *in* Posey, H.H., and Kyle, J.R., eds., Chemical Geology, p. 173-188.

Roberts, H.H., 2001, Fluid and gas expulsion on the northern Gulf of Mexico continental slope; mud-prone to mineral-prone responses, American Geophysical Union Geophysical Monograph, v. 124, 145-161 p.

Roberts, H.H., Aharon, P., Carney, R., Larkin, J., and Sassen, R., 1990, Sea floor responses to hydrocarbon seeps, Louisiana continental slope: Geo-Marine Letters, v. 10, no. 4, p. 232-243.

Roberts, H.H., and Carney, R.S., 1997, Evidence of episodic fluid, gas, and sediment venting on the northern Gulf of Mexico continental slope: Economic Geology v. 92, no. 7/8, p. 863-879.

Ruppel, C., 1997, Anomalously cold temperatures observed at the base of the gas hydrate stability zone on the US Atlantic passive margin: Geology, v. 25, no. 8, p. 699-702.

---, 2000, Thermal state of the gas hydrate reservoir, *in* Max, M.D., ed., Natural Gas Hydrate In Oceanic and Permafrost Environments: Dordrecht, Netherlands (NLD), Kluwer Academic Publishers, p. 29-42.

Ruppel, C., Dickens, G.R., Castellini, D.G., Gilhooly, W., and Lizarralde, D., 2005, Heat and salt inhibition of gas hydrate formation in the northern Gulf of Mexico: Geophysical Research Letters, v. 32, p. 1-4.

Sager, W.W., Lee, C.S., Macdonald, I.R., and Schroeder, W.W., 1999, High-frequency near-bottom acoustic reflection signatures of hydrocarbon seeps on the Northern Gulf of Mexico continental slope: Geo-Marine Letters, v. 18, no. 4, p. 267-276.

Sager, W.W., MacDonald, I.R., and Hou, R., 2003, Geophysical signatures of mud mounds at hydrocarbon seeps on the Louisiana continental slope, northern Gulf of Mexico: Marine Geology, p. 97-132.

Sager, W.W., MacDonald, I.R., Hou, R., Sager, W.W., Bryant, W.R., and Doyle, E.H., 2004, Side-scan sonar imaging of hydrocarbon seeps on the Louisiana continental slope: AAPG Bulletin, v. 88, no. 6, p. 725-746.

Salvador, A., 1991, Origin and development of the Gulf of Mexico Basin, *in* Salvador, A., ed., The Gulf of Mexico Basin: Boulder, Colorado, Geological Society of America, The Geology of North America, v. J, p. 389-444.

Sloan, E.D., Jr., 1998, Clathrate hydrates of natural gases (second ed.): New York, Marcel Dekker Inc., 705 p.

Snyder, F.F.C., Muller, L.K., Dutta, N., Hutchinson, D.R., Hart, P.E., Lee, M.W., Dugan, B., Ruppel, C., Woods, W.T., Coffin, R., Evans, R., and Jones, E.H., 2004, Seismic Analysis and Characterization of Gas Hydrates in the Northern Deepwater Gulf of Mexico AAPG Bulletin v. 88, No. 13 (Supplement), http://www.searchanddiscovery.com/documents/abstracts/annual2004/Dallas/Snyder.htm.

Suter, J.R., and Berryhill, H.L., Jr., 1985, Late Quaternary shelf-margin deltas, Northwest Gulf of Mexico: AAPG Bulletin, v. 69, no. 1, p. 77-91.

Trehu, A.H., Long, P.E., Torres, M.E., Bohrmann, G., Rack, F.R., Collett, T.S., Goldberg, D.S., Milkov, A.V., Riedel, M., Schultheiss, P., Bangs, N.L., Barr, S.R., Borowski, W.S., Claypool, G.E., M.E., D., Dickens, G.R., Gracia, E., Guerin, G., Holland, M., Johnson,

J.E., Lee, Y.J., Liu, C.S., Su, X., Teichert, B., Tomaru, H., Vanneste, M., Watanabe, M., and Weinberger, J.L., 2004a, Three-dimensional distribution of gas hydrate beneath southern Hydrate Ridge: constraints from ODP Leg 204: Earth and Planetary Science Letters, v. 222, p. 845-862.

Trehu, A.M., Flemings, P.B., Bangs, N.L., Chevallier, J., Gracia, E., Johnson, J.E., Liu, C.S., Liu, X., Riedel, M., and Torres, M.E., 2004b, Feeding methane vents and gas hydrate deposits at south Hydrate Ridge: Geophysical Research Letters, v. 31, p. 1-4, doi: 10.1029/2004GL021286.

Tripsanas, E.K., Bryant, W.R., and Phaneuf, B.A., 2004, Depositional processes of uniform mud deposits (unifites), Hedberg Basin, northwest Gulf of Mexico: new perspectives: AAPG Bulletin, v. 88, no. 6, p. 825-840.

Twichell, D.C., Nelson, H., and Damuth, J.E., 2000, Late-stage development of the Bryant Canyon turbidite pathway on the Louisiana continental slope: GSCSEPM Foundation 20th Annual Research Conference, "Deep Water Reservoirs of the World, Dec. 3-6, 2000" (CD Publication), p. 1032-1044.

Whelan, J.K., Eglington, L., Cathles, L.I., Losh, S.L., and Roberts, H., 2005, Surface and subsurface manifestations of gas movement through a N-S transect of the Gulf of Mexico: Marine and Petrol. Geol., v. 22, p. 479-497.

Wilson, A., and Ruppel, C., submitted, Ups and Downs in the Northern Gulf of Mexico: implications of salt tectonics for shallow subseafloor fluid convection: Geology, 15 pp.

Winker, C.D., and Booth, J., 2000, Sedimentary dynamics of the salt-dominated continental slope, Gulf of Mexico: integration of observations from the seafloor, near-surface, and deep subsurface: GCSSEPM Foundation 20th Annual Research Conference, Deep-water Reservoirs of the World, p. 1059-1086 (CD-ROM publication).

Xu, H., Dai, J., Snyder, F., and Dutta, N., 2004, Seismic detection and quantification of gas hydrates using rock physics and inversion, in Taylor, C.E., and Kwan, J.T., eds., Advances in the Study of Gas Hydrates: New York, Kluwer, p. 117-139.

Yu, Z., Lerche, I., and Lowrie, A., 1992a, Thermal impact of salt; simulation of thermal anomalies in the Gulf of Mexico, *in* Schmitz, D.W., Swann, C.T., and Walton, K., eds., Transactions - Gulf Coast Association of Geological Societies, vol.42, p. 381-387.

Yu, Z., Lerche, Y.I., and Lowrie, A., 1992b, Thermal impact of salt; simulation of thermal anomalies in the Gulf of Mexico: Pure and Applied Geophysics, v. 138, no. 2, p. 181-192.

Figure Captions

Figure 1: A – Shaded-relief bathymetry of the Gulf of Mexico (taken from NOAA Coastal Relief Model); box shows location of Figure 1B. B – Slope map of the area in the vicinity of the Casey minibasin; slope map created from NOAA Coastal Relief Model of the Gulf of Mexico; box shows location of Figure 1C. C – Bathymetric map of the study area. Tan colors are shaded-relief bathymetry from the NOAA Coastal Relief Model for the Gulf of Mexico. Colored box shows bathymetry taken from 3D mcs data. Locations of seismic lines (green) and heat flow stations (blue circles), and JIP research well (red star) are shown, together with geologic features.

Figure 2: Line KC01 migrated seismic data. Location is shown in Figure 1C. Lower section shows heat flow measurement positions (HF), major unconformity (U), faults (solid lines), BSR (red arrows), bright spots and the chimney beneath the Beta mound.

Figure 3: Line KC11 migrated seismic data. Location is shown in Figure 1C. Lower section shows heat flow measurement positions (HF), faults (solid lines), and BSR (red arrows).

Figure 4: Line KC57 migrated seismic data. Location is shown in Figure 1C. Lower section shows heat flow measurement positions (HF), faults (solid lines), BSR (red arrows), and the chimney beneath the Beta mound. A second chimney/seep site may exist near CDP 2350.

Figure 5: A – 3D multichannel seismic reflection profile showing reflections in the Casey basin, a major unconformity (U), the East Casey fault zone, the BSR (black arrows), and the Beta mound. B – Enlargement of the region of the BSR showing the alternating bright spots associated with the BSR. These brighter reflections are interpreted as coarser units that contain free-gas deposits.

Figure 6: Evidence for salt in and around the Casey minibasin. A – 3D seismic section from within the study area showing example of the salt reflection. B – Contoured map of the top of salt (transparent white region with white to black contours); contour interval is .2 s. Dashed line around the salt indicates limit of the data. The shape and geometry of the top-of-salt surface is

not reflecting a water bottom effect: travel times to the sea floor (orange contours) change a maximum of .25 s; travel time to the top of salt vary by about .5 s. Red star marks the location of the JIP research well.

Figure 7: A – Map showing extent and depth to BSR, superimposed over map shown in Figure 1C. Thick black line delineates the mapped boundary of the BSR. This black lines are contours in meters below the sea surface. Red star shows location of JIP drilling completed in Spring, 2005. B – Map showing amplitude anomalies from 3D multichannel data. The dashed line shows the limit of the 3D multichannel data used in mapping the BSR. Faults from Figure 1C are also shown.

Figure 8: Thermal gradient information. Profiles of gradient values at the heat flow stations are shown along KC01 (A) and KC11 (B). C. Boundary between the two regimes of higher gradients (on the northeast) and lower gradients (on the southwest) superimposed on the map shown in Figure 1C.

Figure 9: P-T diagram showing the theoretical methane-seawater phase boundary (heavy line) with the estimated BSR temperatures (circles) calculated from extrapolation of thermal gradients measured with conventional heat flow methods and adopting BSR depths (cast as hydrostatic pressures) based on the 3D MCS data. Error bars are included on the BSR temperature estimates by propagating the uncertainties from the original thermal gradient data.

Figure 10: Conceptual models to explain temperature discrepancies. In each case, the top panel shows a schematic of the hydrologic or geologic process and the bottom panel demonstrates the impact on the measured (thick dashed line) and actual (gray line) geotherms. A – Downward advection of cooler seawater. For this case, the actual gradient is concave upwards and the heat flow penetration only samples the upper, linear portion of the curve. B –Rapid sedimentation/mass wasting. For this case, three of the lines indicate (i) gradient at the time of deposition $(dT/dz)_0$, (ii) gradient at the present time (actual gradient), and (iii) gradient at the

future equilibrium state $(dT/dz)_{equil}$. The heat flow penetration samples a thermal condition that appears to be in equilibrium, but is not the actual gradient (gray line). C—Thermal focusing at depth due to the presence of high thermal conductivity salt. For this case, the heat flow penetration would only have sampled the near-seafloor portion of the actual thermal profile.

Figure 11: Relationship between temperature misfit and travel time to top of salt. The lack of a linear (or other obvious) relationship between these two variables suggests that salt is not the explanation for why thermal gradients measured at the sea floor are too low when extrapolated to depth (as proposed in the scenario illustrated in Figure 10C).

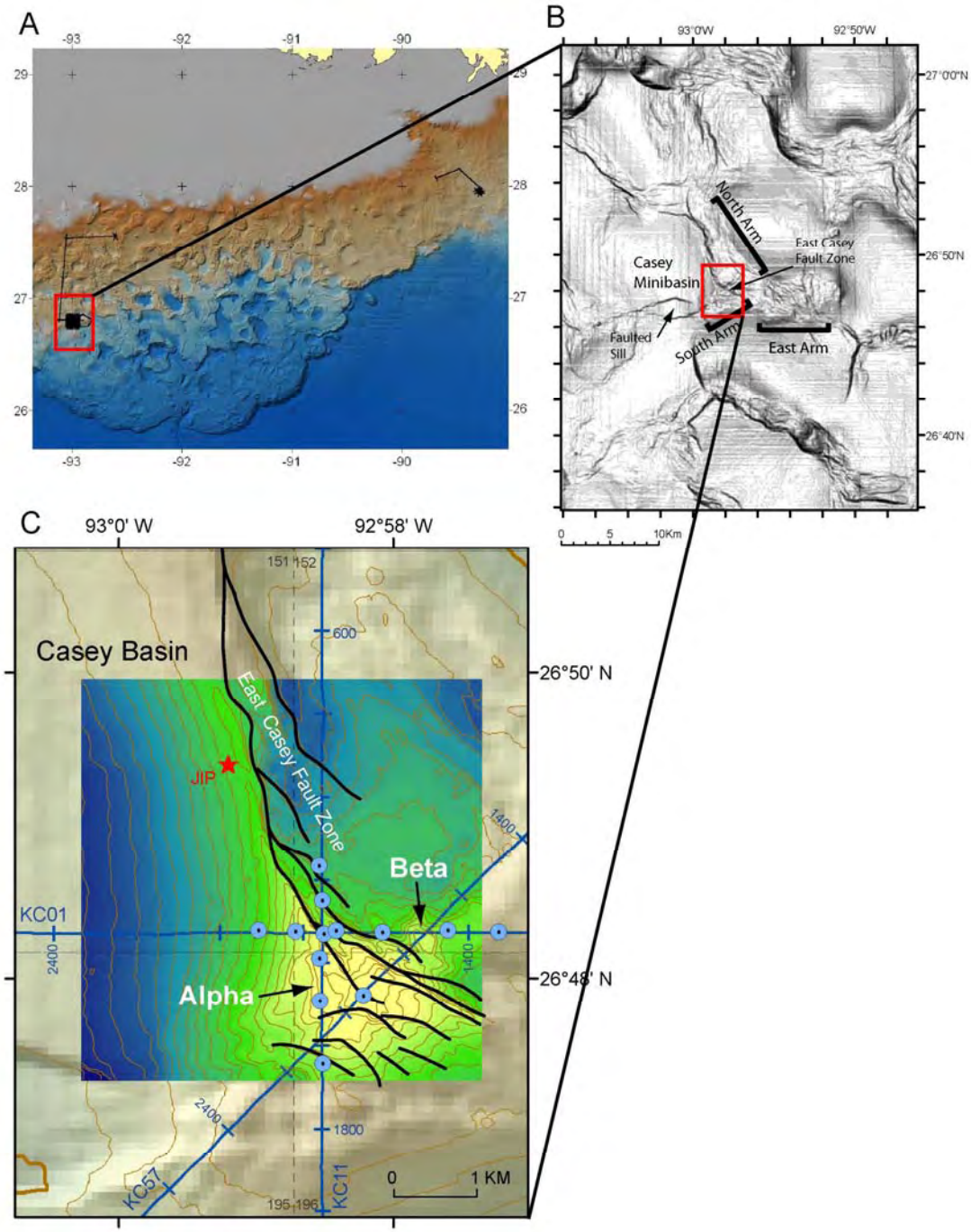

Figure 1 Hutchinson and others, Hedberg

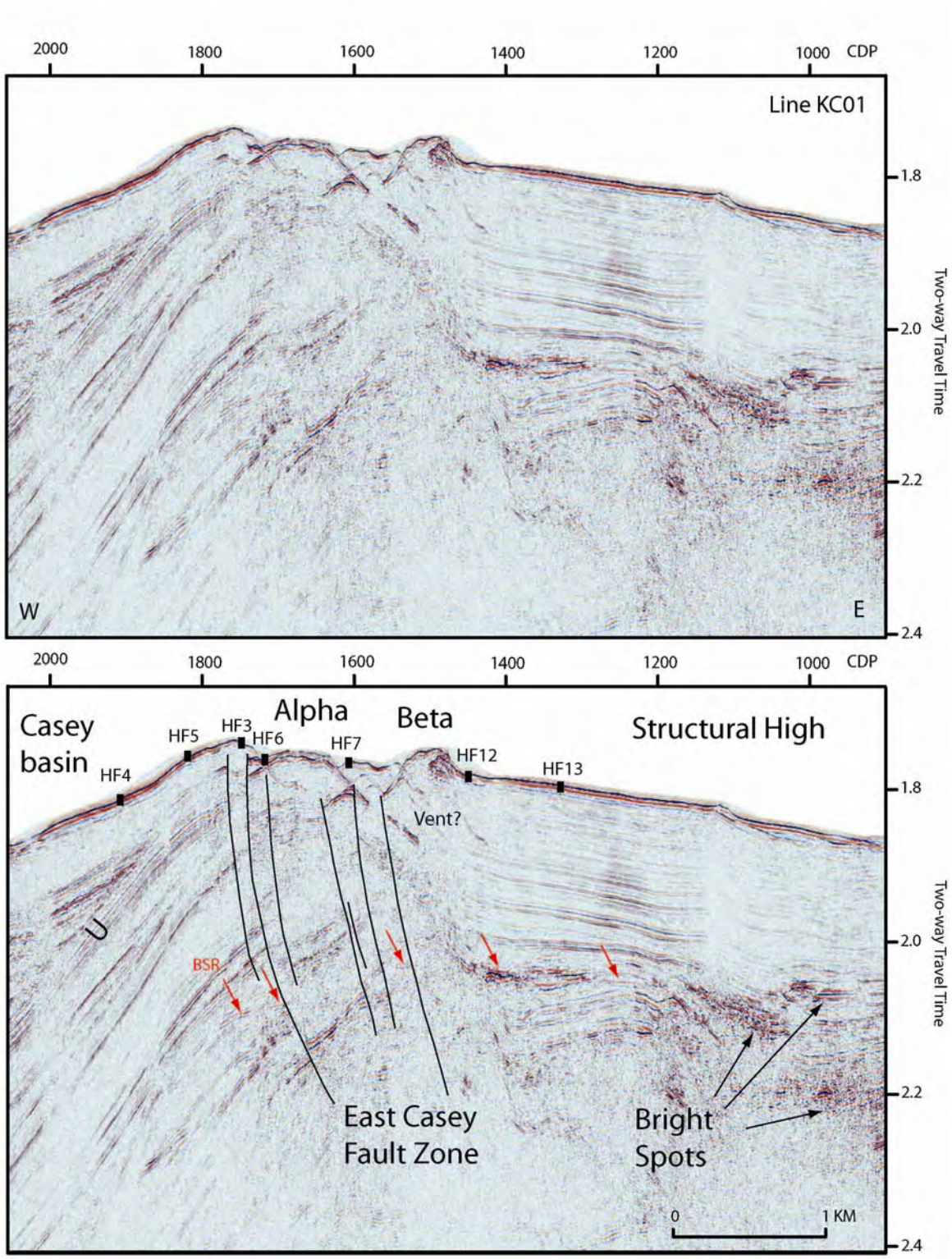

Figure 2 Hutchinson and others, Hedberg

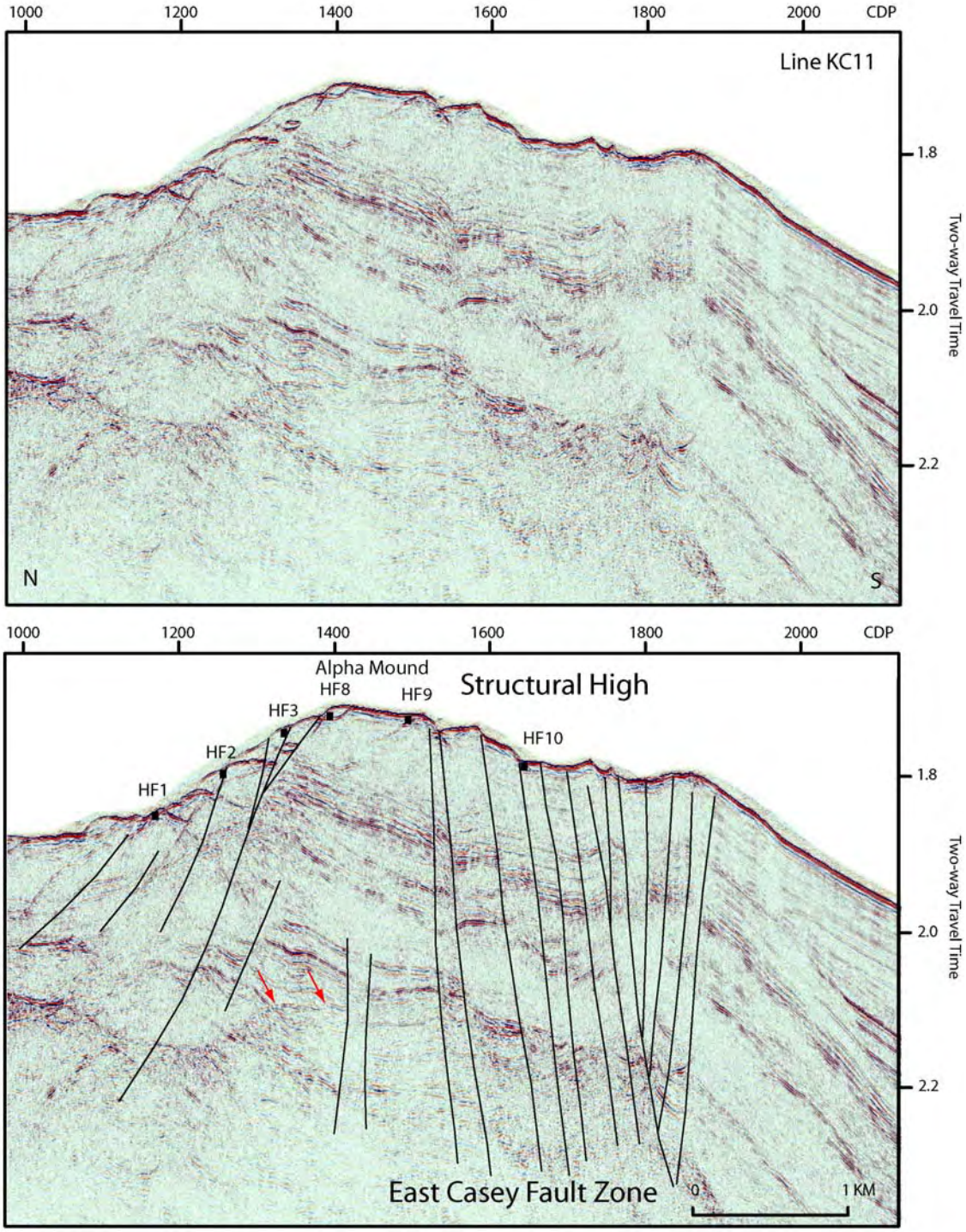

Figure 3 Hutchinson and others, Hedberg

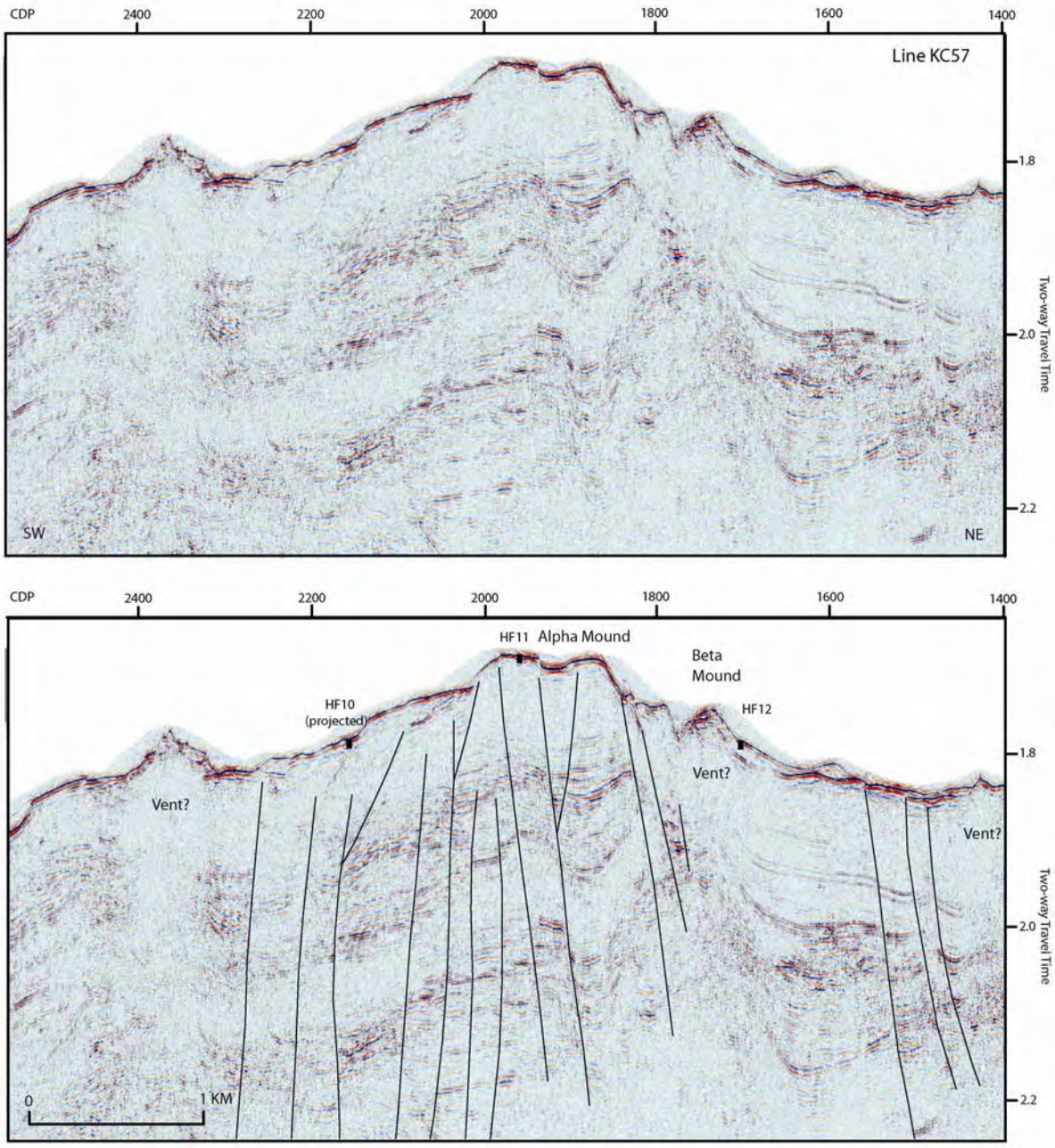

Figure 4 Hutchinson and others, Hedberg

A. 3D Multichannel Seismic Profile

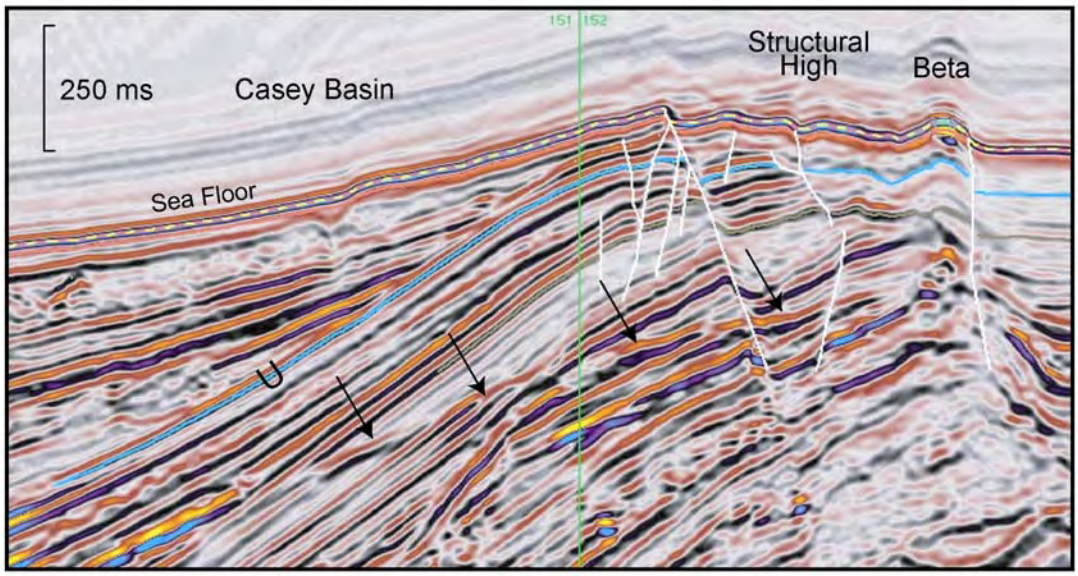

B. High-Resolution 3D Image of BSR

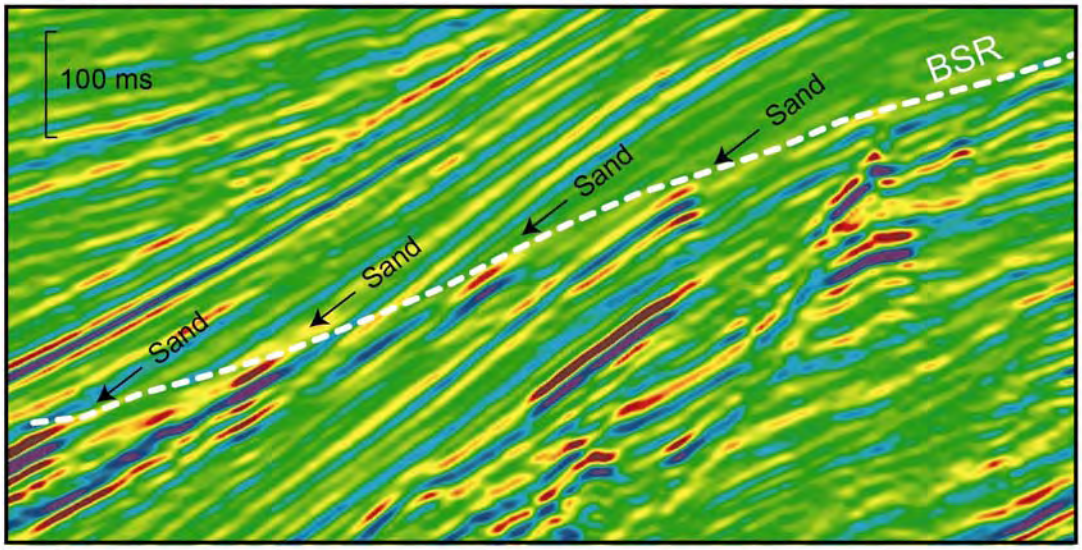

Figure 5 Hutchinson and others, Hedberg

A. Salt Reflection

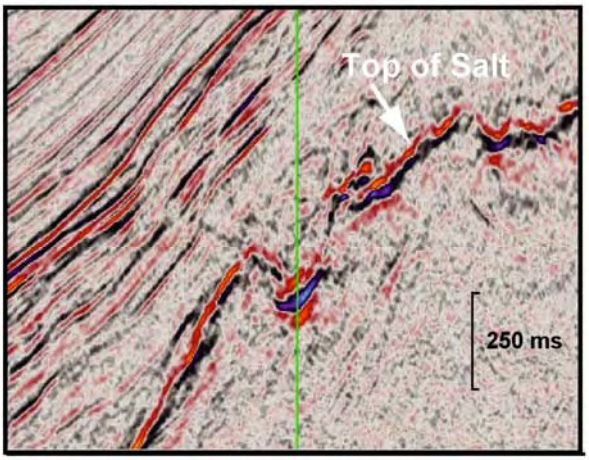

B. Salt Map

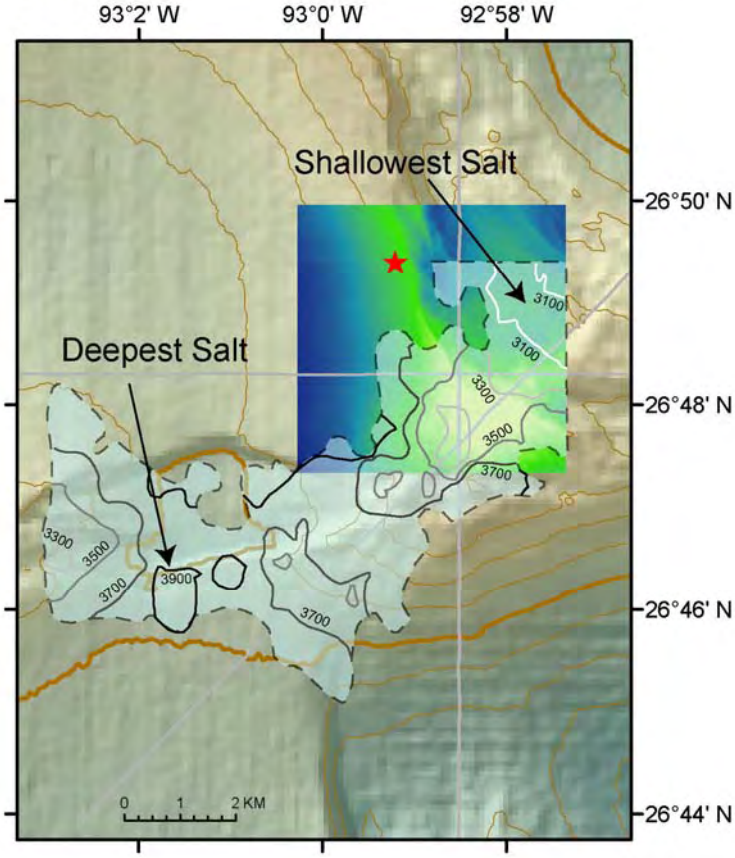

Figure 6 Hutchinson and others, Hedberg

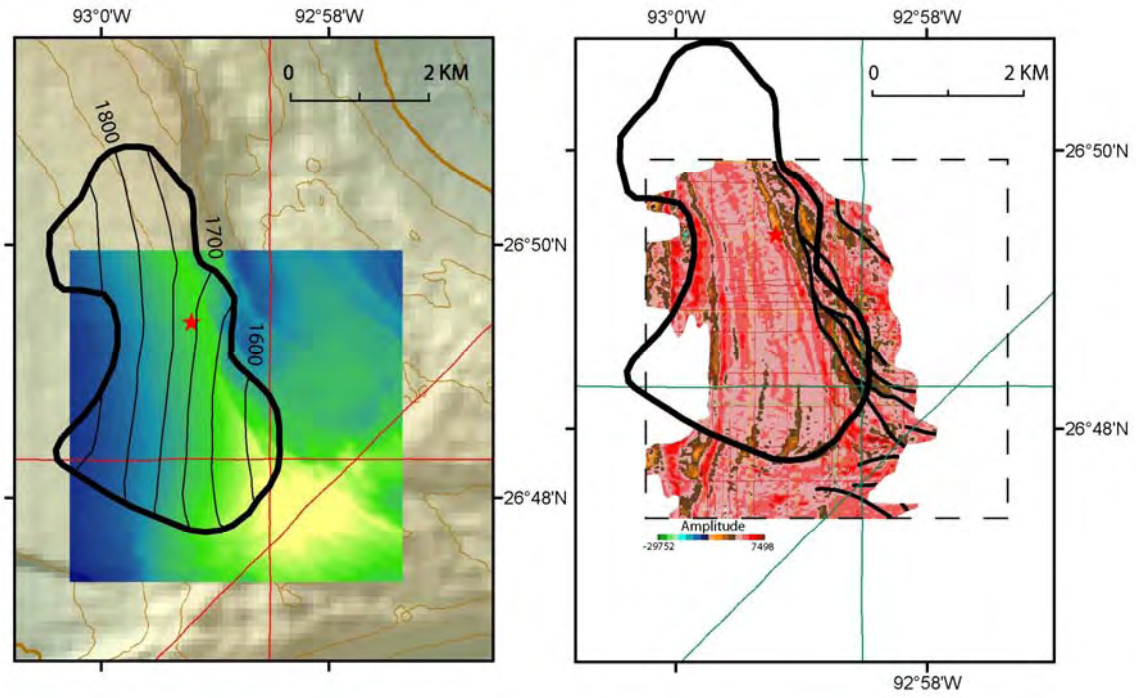

Figure 7 Hutchinson and others, Hedberg

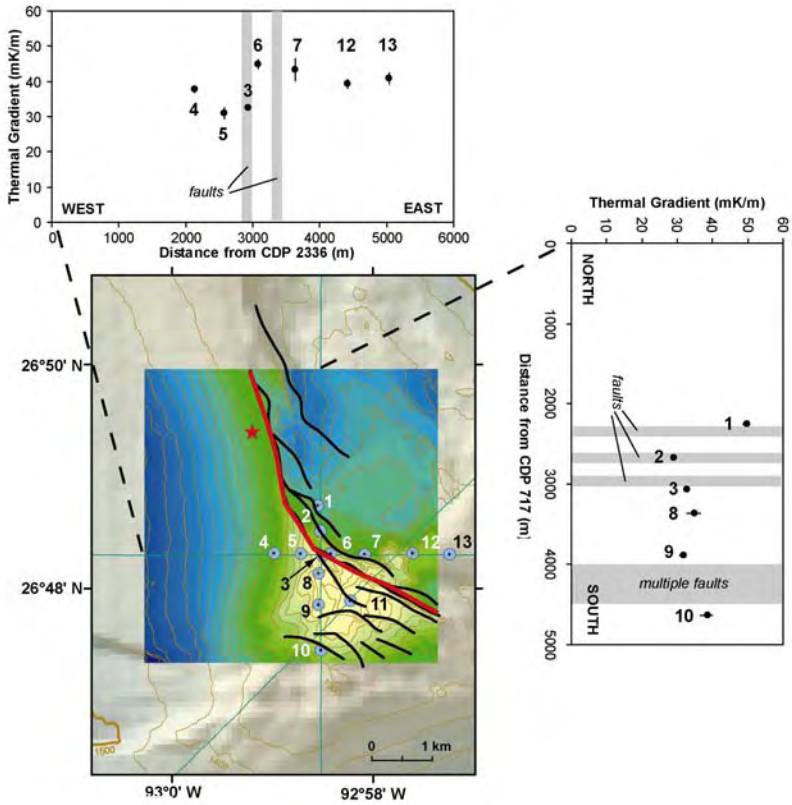

Figure 8 Hutchinson and others, Hedberg

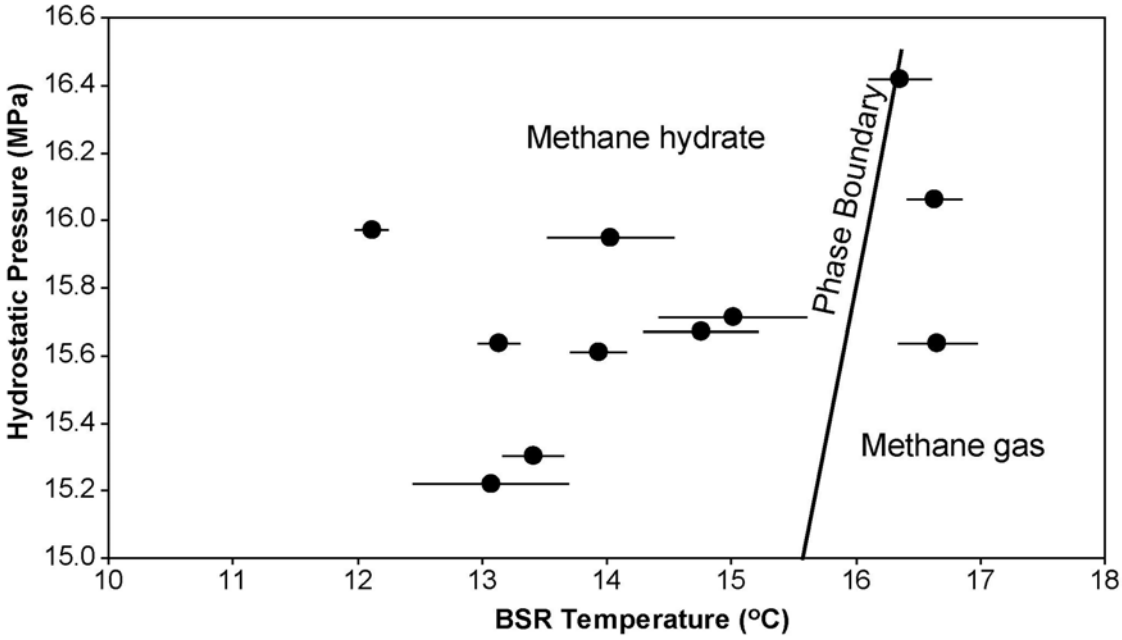

Figure 9 Hutchinson and others, Hedberg

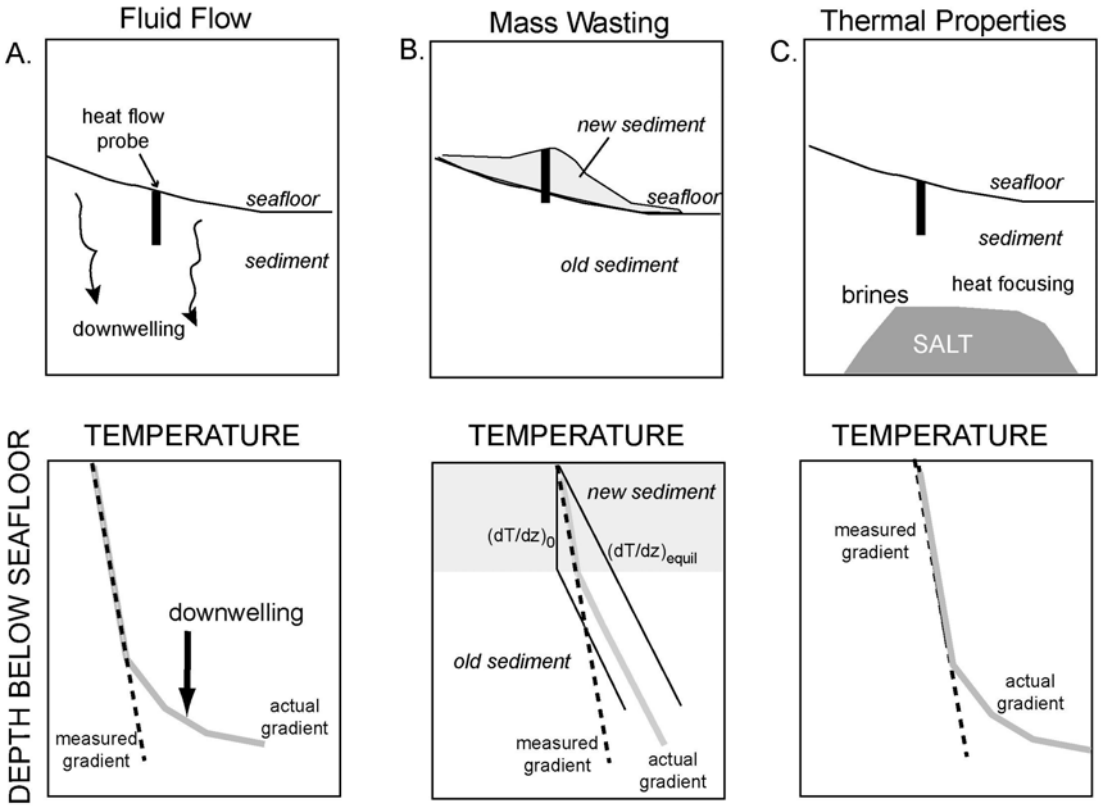

Figure 10 Hutchinson and others, Hedberg

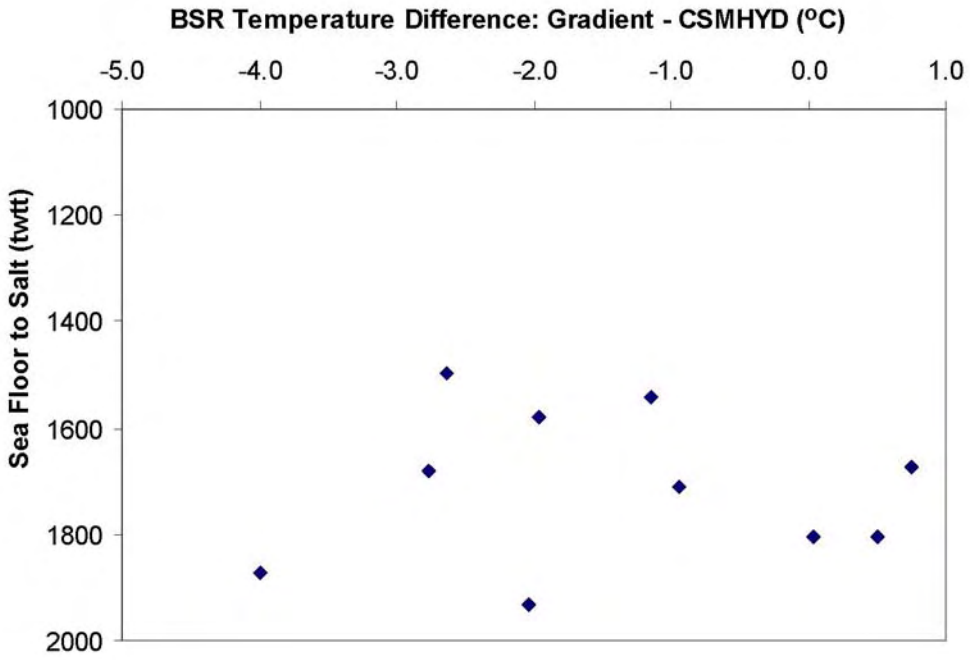

Figure 11 Hutchinson and others, Hedberg